Research Square

Preprints are preliminary reports that have not undergone peer review.
They should not be considered conclusive, used to inform clinical practice,
or referenced by the media as validated information.

Continuity, not peak signal, should guide flip-angle optimization of slow-flow vertebral artery V3

Guijin Li
Beijing Chaoyang Hospital, Capital Medical University
Jiewen Qiu
Tingzhou Hospital
Dianjiang Zhao
Beijing Chaoyang Hospital, Capital Medical University
Hongjie Cao
Beijing Chaoyang Hospital, Capital Medical University
Xiuqin Jia
Beijing Chaoyang Hospital, Capital Medical University
Haishui Xie
Tingzhou Hospital
Shuitao Qiu
Tingzhou Hospital
Qi Yang
yangyangqiqi@gmail.com

Beijing Chaoyang Hospital, Capital Medical University

Research Article

Keywords:

Posted Date: November 19th, 2026

DOI: https://doi.org/10.21203/rs.3.rs-11622771/v1

License: This work is licensed under a Creative Commons Attribution 4.0 International License.
Read Full License

Additional Declarations: No competing interests reported.

Abstract

Background and Purpose

Three-dimensional time-of-flight MR angiography of the slow-flow vertebral artery V3 is conventionally optimized by maximizing signal-to-noise ratio or contrast-to-noise ratio, whether these indices predict reader-assessed depiction of a long, tortuous segment is unknown. We tested whether flip angle optimization guided by peak signal-to-noise ratio or contrast-to-noise ratio identifies the best V3 depiction and which metric drives reader-assessed depiction.

Materials and Methods

In this prospective study, 38 participants (21 women, 17 men; mean age 50.9 ± 11.3 years) underwent cervical 3D time-of-flight MR angiography at eight center flip angles (8°–25°; 18° routine) with otherwise identical parameters acquired in randomized order. Reader-assessed V3 depiction, signal-to-noise ratio, contrast-to-noise ratio, contrast-to-background ratio, the vertebral artery V3/internal carotid artery C3 ratio and proximal-to-distal V3 decay were measured; correlations and flip-angle × dominance interactions were analyzed.

Results

Vertebral artery V3 signal-to-noise ratio peaked at 16° (≈ 446) with no significant difference across 12°–20°, reader score fell from 12° and reader-assessed diagnostic adequacy dropped from 100% at 12° to 71.8% at 16° and 41.0% at 18° (both $p < 0.01$ versus 12°). Decay rose monotonically (8.4%–50.6%), exceeding 25% where scores collapsed. Reader score correlated with continuity (vertebral artery V3/internal carotid artery C3 ratio $\rho \approx 0.61$, decay $\rho \approx -0.62$) far more strongly than with signal-to-noise ratio ($\rho \approx 0.19$) or contrast-to-noise ratio ($\rho \approx 0.12$; 95% confidence interval includes 0).

Conclusions

For slow-flow vertebral artery V3, optimizing flip angle by peak signal-to-noise ratio or contrast-to-noise ratio is inadequate because these indices ignore intra-slab saturation; along-segment continuity which is quantified by proximal-to-distal decay or the vertebral artery V3/internal carotid artery C3 ratio and governed by Bloch recurrence is the endpoint that tracks reader depiction. A lower flip angle (approximately 12°) preserves V3 continuity without compromising fast-flow depiction. Reader-assessed V3 depiction scores peaked at 12° (4.75 ± 0.72) with 100% diagnostic adequacy, declining to 41.0% at 18° ($p < 0.01$ versus 12°).

Introduction

Three-dimensional time-of-flight (3D TOF) MR angiography is the workhorse for non-contrast imaging of the cervical vertebral artery (VA). Among its adjustable parameters, the excitation flip angle (FA) governs vessel signal and conspicuity. Conventional protocol design optimizes the FA to maximize vessel signal-to-noise ratio (SNR) or contrast-to-noise ratio (CNR), following the Ernst-angle principle that a single, often large, FA best recovers steady-state signal [1] [2] [3]. Cervical 3D TOF protocols therefore commonly default to a relatively high FA (18°–25°) [4].

To compensate intra-slab saturation, modern 3D TOF employs tilted optimized non-saturating excitation (TONE), which ramps the FA along the slab to keep steady-state signal more uniform [5] [6] [7]. TONE mitigates but does not abolish in-plane saturation, and the FA is often chosen to maximize SNR or CNR, a strategy known as the Ernst-angle prescription [1] [2] [3]. Empirical optimization studies have likewise selected the highest-SNR FA, predominantly for fast-flow intracranial vessels or short through-plane segments [8] [9]. Whether an SNR/CNR-optimal FA remains optimal for a long, slow-flow vessel such as V3 has never been tested.

This logic assumes that the ROI-averaged SNR is a faithful proxy for diagnostic depiction. It breaks down for the VA V3 segment. V3 is a long, tortuous [10] [11], intrinsically slow-flow vessel; as blood traverses the slab, it is repeatedly excited and progressively saturates, so signal decays from proximal to distal [5] [6] [7] which is a recognized property of the vertebral artery V3 segment [12]. A high FA accelerates this saturation, and the resulting V3 dropout is invisible to a mean SNR over the whole vessel. In practice, readers judge V3 by whether the segment remains visible from end to end, which depends on continuity rather than on peak or mean SNR.

Whether peak SNR/CNR predicts V3 depiction has never been tested, and the correct endpoint for a long slow-flow vessel remains undefined with direct consequences for 3D TOF protocol tuning. Using a cohort scanned at eight center FAs, we asked: (I) does peak-SNR/CNR optimization identify the FA readers judge best; (II) which metric tracks depiction and (III) why slow-flow V3 diverges from fast-flow segments such as the ICA, and whether vertebral dominance modifies the answer.

Materials and methods

Study population

This single center prospective study was approved by the Institutional Review Board of the authors' institution (approval number withheld for double-blind review) and written informed consent was obtained from all participants. All procedures were performed in accordance with the ethical standards of the institutional and national research committees and with the 1964 Declaration of Helsinki and its later amendments. This is a planned companion analysis of the same prospective 3D time-of-flight MR angiography flip-angle cohort as a manuscript currently under review, which addresses the distinct clinical question of estimating the optimal FA for V3 depiction and comparing it with clinical routine 18°. Between November 2025 and September 2026, 356 subjects screened for cervicocranial MR

angiography were reviewed; 57 consented and 38 completed all eight flip-angle acquisitions, forming the final cohort. Of these 38 (17 men, 21 women; mean age = 50.9 ± 11.3 years, range 28–79), all had complete bilateral V3 signal-to-noise ratio and formed the primary quantitative sample, and all contributed to reader-assessed depiction and diagnostic adequacy (Fig. 1). Inclusion criteria were age ≥ 18 years, no MR contraindication and clinical suspicion of intracranial ischemia or vertebrobasilar insufficiency; exclusion criteria were stent or prior vascular surgery affecting the evaluation and incomplete or non-diagnostic acquisitions.

Image acquisition

All scans were performed on a 3.0T MR system (vendor withheld for double-blind review) with a 20-channel neck coil. A 3D TOF MRA sequence was repeated eight times in the same session at centerFAs of 8°, 10°, 12°, 14°, 16°, 18°, 20° and 25° (acquisition order randomized by a random permutation of the eight FAs within each participant); the routine clinical setting was 18°. Each scanning used an identical parameter, so differences reflect FA alone. Tilted optimized non-saturating excitation (TONE) was applied at 70% (inflow-to-outflow slab-edge flip-angle ratio; the reported FA is the slab center). Other parameters were identical across FAs: 22/3.69/1 (TR/TE/Average), FOV = 230 × 230 mm, matrix = 256 × 225, slice thickness = 1.0 mm, voxel size = 0.9 × 1.0 × 1.0 mm^3, parallel imaging factor = 2, bandwidth = 250 kHz; the transverse slab covered the cervical spine from the upper aortic arch to the circle of Willis, with a saturation band to suppress venous signal. Total acquisition time per FA was 5 min 11 s.

Image analysis

Qualitative analysis

Images were anonymized as to FA and loaded onto a post-processing workstation (vendor withheld for double-blind review). Two board-certified radiologists (15 and 6 years of cardiovascular MRI experience) who were received standardization training independently scored overall image quality and depiction of the VA V2 and V3 segments, the ICA-C3 segment and the common carotid origin on a 5-point scale (1 = not visible; 2 = partially visible; 3 = visible but clearly lower in signal; 4 = visible but slightly lower; 5 = signal equal to other segments). A V3 score ≥ 4 was defined as diagnostic adequacy; reader-assessed diagnostic adequacy was the proportion of participant–flip-angle combinations rated diagnostic by reader 1. For diagnostic adequacy the analytic unit was the participant–flip-angle combination; with 38 participants and 8 flip angles this yielded 304 combinations per side (296 on the right after excluding 8 non-physical SNR pairs). Reader 1 provided complete ratings for all 38 participants.

Quantitative analysis

A third radiologist (8 years of cardiovascular MRI experience, blinded to FA) placed regions of interest on the V3, V2, ICA-C3 and common carotid origin. SNR, CNR and CBR were computed, contrast-to-background ratio (CBR) used the sternocleidomastoid muscle as background. The following metrics

were derived: SNR=blood signal intensity (SI) / background SD; CNR= (blood SI − muscle SI) / background SD and CBR= (blood SI − muscle SI) / muscle SI. The V3/ICA-C3 signal ratio was the V3-to-ICA-C3 SNR ratio. Along-segment continuity was quantified as the proximal-to-distal V3 signal decay rate, (SI_proximal − SI_distal)/SI_proximal × 100%, measured on source images at the proximal and distal ends of V3, defined anatomically as the segment at the C1–C2 level and at the dural entry/foramen magnum, respectively.

Statistical analysis

Normality was assessed (Shapiro–Wilk). Differences across the eight flip-angles were tested with repeated-measures ANOVA (Greenhouse–Geisser correction) for continuous metrics and the Friedman test for reader scores; the routine 18° was the reference in Wilcoxon signed-rank comparisons with Holm correction. The association between reader V3 score and each quantitative metric was assessed with exploratory Spearman correlation, because each participant contributed 16 non-independent pairs (8 flip-angles × 2 sides); 95% CIs were obtained by a participant-clustered bootstrap (2,000 resamples). Reader-assessed diagnostic adequacy across FAs was modeled with generalized estimating equations (GEE; binomial family, exchangeable working correlation, clustered by participant), with participant-level McNemar tests for prespecified pairwise contrasts. Odds ratios were not estimable at 12° (38/38 diagnostic) and 25° (0/38 diagnostic) because of quasi-complete separation; we therefore report the GEE omnibus p with McNemar pairwise contrasts. A linear mixed model with subject as random intercept tested the flip-angle × vertebral-dominance interaction, with balanced-dominance participants (n = 25) included as a third dominance level. Given the within-subject design and large effect sizes (partial η^2 up to 0.90), flip-angle effects were robustly detectable at n = 38; no post hoc power was calculated. Analyses used IBM SPSS Statistics version 26.0 (IBM Corp., Armonk, NY, USA); $p < 0.05$ denoted significance. The study was reported in line with the STROBE statement [13].

Results

Of 356 screened subjects, 57 consented and 38 completed all eight FAs acquisitions, forming the final cohort (Fig. 1); baseline characteristics are summarized in Table 1. One side in one participant was non-visualized at all FAs and treated as missing; that side was excluded from side-specific paired analyses.

Table 1
Baseline characteristics of the quantitative sample (n = 38).

Characteristic	Value
Age (years), mean ± SD	50.9 ± 11.3
Age range (years)	28–79
Male, n (%)	17 (44.7)
Female, n (%)	21 (55.3)
Vertebral artery dominance: balanced, n (%)	25 (65.8)
Vertebral artery dominance: left-dominant, n (%)	10 (26.3)
Vertebral artery dominance: right-dominant, n (%)	3 (7.9)
Enrolment period	November 2025 – September 2026
SD, standard deviation.	

Peak SNR is highest where depiction fails

Inter-reader agreement was excellent (quadratic-weighted κ = 0.98 bilaterally; all items κ ≥ 0.80). V3 SNR peaked at 16° (446.4 ± 98.8) with a plateau across 12°–20° (408–446) and did not differ significantly from the peak in that range (Holm-corrected $p > 0.05$; 12° versus 16°, $p = 0.08$). Reader score had already fallen significantly by 16° (− 0.86 versus 12°, 95% CI − 1.05 to − 0.66, $p < 0.001$) and reader-assessed diagnostic adequacy dropped from 100% (95% CI 91.0–100.0) at 12° to 71.8% (56.2–83.5) at 16° and 41.0% (27.1–56.6) at 18° (GEE clustered by participant: overall $p < 0.001$; McNemar versus 12°: $p = 1.95 \times 10^{-3}$ and $p = 4.77 \times 10^{-7}$) (Fig. 2). The FA that maximizes mean SNR doesn't maximize the V3 depiction. The standard Ernst logic would select ≈ 16° as FA, but at this angle readers judged V3 to be a suboptimal depiction. Representative angiograms illustrate this dissociation (Fig. 3): distal V3 continuity is lost at routine 18° but preserved at 12° (Fig. 3a, b).

Reader-assessed V3 depiction peaks at 12° across the full 8°–25° range

Reader-assessed V3 depiction score (mean of two blinded raters, both sides pooled) described an inverted-U across the full 8°–25° range, peaking at 12° (4.75 ± 0.72) and declining monotonically thereafter (14°, 4.58 ± 0.87; 16°, 3.92 ± 1.03; 18°, 3.17 ± 1.15; 25°, 1.43 ± 0.76; Fig. 4a, Supplementary Table 1). Diagnostic adequacy was 100% at 10°–12° and 94.9% at 14° but fell below the 85% adequacy threshold at 16° (71.8%) and collapsed to 41.0% at 18° and ≤ 7.7% at ≥ 20° (Fig. 4b). Overall image quality and segment continuity followed the same pattern, with maximum at 12° (4.88 and 4.87, respectively). The V3/ICA-C3 signal ratio declined monotonically with FA and fell below unity beyond 18° (0.99 at 18°, 0.73 at 25°), indicating that the distal V3 signal drops below the cervical background despite globally

brighter vessel signal (Supplementary Table 1). Full per-flip-angle reader scores, overall image quality, segment continuity, diagnostic adequacy, and V3/ICA-C3 signal ratios are provided in Supplementary Table 1.

Continuity, not peak signal, tracks depiction

The proximal-to-distal V3 decay rate rose monotonically with FA, from 8.4% at 8°, 15.1% at 10° and 17.9% at 12° to 24.9% at 14°, 31.0% at 16°, 36.5% at 18°, 41.0% at 20° and 50.6% at 25° (Friedman $\chi^2 = 252.8$, $p < 0.001$, Kendall $W = 0.950$; Table 2). Decay tended to exceed ≈ 25% in the same flip-angle range where reader metrics fell most steeply; we therefore flag ≈ 25% only as an illustrative, cohort-derived decay level (exploratory), not a validated threshold (Fig. 2a). Exploratory Spearman correlation supported the pattern: reader V3 score correlated strongly and significantly with the continuity metrics, the V3/ICA-C3 ratio (pooled $\rho = 0.61$, 95% CI 0.54–0.68) and decay rate ($\rho = -0.62$, 95% CI − 0.68 to − 0.54), weakly with V3 SNR ($\rho = 0.19$, 95% CI 0.09–0.29) and, after clustering adjustment, not significantly with CNR ($\rho = 0.12$, 95% CI 0.00–0.22) or usefully with CBR ($\rho = -0.04$, 95% CI − 0.21 to 0.13; Table 3, Fig. 5b). Optimizing by peak SNR or CNR thus overestimates the optimal FA because these indices ignore along-segment loss (the mechanism quantified in Fig. 6). Table 3 and Fig. 5b make the dissociation explicit: among all candidate metrics only the two continuity measures, the V3/ICA-C3 ratio and the decay rate carried a strong, consistent correlation with reader score, whereas CBR, which rises with FA purely through background suppression, showed limited utility in this context.

Table 2
Quantitative metrics of the vertebral artery V3 segment across FAs (n = 38).

Flip angle	V3 SNR	V3 CNR	V3 CBR	V3/ICA-C3 ratio	Decay rate (%)
8°	339.6 ± 89.7	183.3 ± 55.0	1.18 ± 0.22	1.25 ± 0.17	8.4 ± 7.8
10°	393.1 ± 88.8	234.7 ± 56.2	1.51 ± 0.26	1.26 ± 0.18	15.1 ± 7.0
12°	407.7 ± 82.4	258.2 ± 61.2	1.74 ± 0.34	1.21 ± 0.19	17.9 ± 7.7
14°	428.8 ± 118.0	285.0 ± 89.1	2.00 ± 0.45	1.15 ± 0.22	24.9 ± 8.3
16°	446.4 ± 98.8	302.6 ± 74.2	2.18 ± 0.56	1.08 ± 0.20	31.0 ± 8.3
18°	416.8 ± 100.0	286.8 ± 84.7	2.27 ± 0.72	0.99 ± 0.22	36.5 ± 8.9
20°	410.5 ± 123.3	285.5 ± 103.5	2.33 ± 0.80	0.92 ± 0.24	41.0 ± 8.9
25°	347.8 ± 94.6	239.2 ± 87.7	2.29 ± 0.97	0.73 ± 0.24	50.6 ± 9.0
F value	9.93	20.32	53.26	186.45	317.78
p (Greenhouse–Geisser)	< 0.001	< 0.001	< 0.001	< 0.001	< 0.001
Partial η^2	0.212	0.355	0.590	0.834	0.896

Data are mean ± SD; one-way repeated-measures ANOVA (df1 = 7, df2 = 259). Decay rate = proximal-to-distal signal loss. CBR, contrast-to-background ratio; CNR, contrast-to-noise ratio; ICA, internal carotid artery; SNR, signal-to-noise ratio.

Table 3
Spearman correlation of reader V3 score with each quantitative metric.

Quantitative metric	Spearman ρ (left)	Spearman ρ (right)	Pooled inference
V3 SNR	0.14	0.24	0.19 (0.09 to 0.29); weak positive
V3 CNR	0.08	0.16	0.12 (0.00 to 0.22); weak, not significant
V3 CBR	-0.06	-0.03	-0.04 (-0.21 to 0.13); not significant
V3/ICA-C3 ratio	0.55	0.68	0.61 (0.54 to 0.68); strong positive
V3 decay rate (%)	-0.65	-0.60	-0.62 (-0.68 to -0.54); strong negative

Reader V3 score is the mean of two blinded raters. Spearman ρ was computed per side and pooled across all reader–metric pairs (n = 304 left / 296 right; 38 participants × 8 flip angles × 1 side each; 8 right-side pairs with non-physical SNR = 0 were excluded). Observation units repeat within participants and are not independent; 95% CIs were derived from a 2,000-replicate participant-clustered bootstrap (participants resampled as clusters). Because this correlation is exploratory, the pooled ρ is reported for direction and rank order rather than as a precise effect size; it combines the left- and right-side analyses and reflects their qualitative agreement. Reader depiction tracks continuity (ratio, decay) but not peak SNR/CNR. CBR, contrast-to-background ratio; CNR, contrast-to-noise ratio; ICA, internal carotid artery; V3, vertebral artery third segment.

V3 diverges from fast-flow segments

Whereas V3 SNR peaked at 16° and fell thereafter, the SNR of V2 and ICA-C3 rose to 25° (ICA-C3 311→609; V2 331→530), with low decay throughout (Table 4, Fig. 2b). The V3/ICA-C3 ratio fell from 1.25 at 8° to 0.73 at 25°, showing that slow-flow V3 saturates at a far lower FA than fast-flow ICA. A single large FA therefore helps fast-flow segments while harming V3; a lower FA preserves V3 continuity and only mildly reduces the still-high SNR of V2 and ICA-C3. Because fast-flow segments keep gaining signal up to 25° while V3 has already saturated, no single large FA served both vessels; the angle that rescues V3 costs a 16–22% SNR reduction in V2 and ICA-C3 relative to 18°. Representative axial MIPs showed preserved intracranial depiction at every FA, including the lowest (Fig. 3c), confirming that the lower FA does not compromise fast-flow intracranial visualization.

Table 4
Segment divergence: SNR of V3 versus fast-flow segments across FAs (n = 38).

Flip angle	V3 SNR	V2 SNR	ICA-C3 SNR	V3/ICA-C3 ratio
8°	339.6 ± 89.7	331.2 ± 93.2	310.7 ± 85.8	1.25 ± 0.17
10°	393.1 ± 88.8	381.6 ± 102.2	365.5 ± 96.3	1.26 ± 0.18
12°	407.7 ± 82.4	419.1 ± 80.1	402.6 ± 83.7	1.21 ± 0.19
14°	428.8 ± 118.0	446.6 ± 121.4	447.9 ± 113.1	1.15 ± 0.22
16°	446.4 ± 98.8	513.5 ± 148.5	516.8 ± 141.1	1.08 ± 0.20
18°	416.8 ± 100.0	499.3 ± 117.3	519.6 ± 115.0	0.99 ± 0.22
20°	410.5 ± 123.3	521.2 ± 151.8	566.6 ± 157.5	0.92 ± 0.24
25°	347.8 ± 94.6	529.8 ± 124.1	609.2 ± 139.5	0.73 ± 0.24

Data are mean ± SD. V3 (slow-flow) peaks at 16° and falls; V2 and ICA-C3 (fast-flow) rise to 25°. SNR, signal-to-noise ratio; ICA, internal carotid artery.

Dominance did not significantly modify the flip-angle optimum

In the 13 dominant type participants, V3 SNR was numerically higher on the dominant vertebral-artery side than on the contralateral non-dominant side (391.7 versus 366.1, difference 25.6) but this difference was not statistically significant ($p = 0.35$; CNR difference 25.2, $p = 0.36$). The flip angle × dominance interaction was non-significant for V3 SNR ($p = 0.86$), CNR ($p = 0.83$), the V3/ICA-C3 ratio ($p = 0.42$) and decay ($p = 0.34$; Table 5, Fig. 5a), indicating no significant dominance × flip-angle interaction; however, subgroup power is limited (13 dominant-type participants, only 3 right-dominant), and this null result should be interpreted cautiously. Vertebral dominance was therefore not associated with a different flip-angle optimum in this cohort. Practically, a single low FA therefore serves balanced, left dominant and right dominant anatomies alike, and no dominance-specific protocol adjustment appeared necessary in this cohort.

Table 5
Vertebral dominance: side comparison and flip-angle × dominance interaction.

Metric	Dominant side	Non-dominant side	Side diff	Side p	FA × dominance p
V3 SNR	391.7	366.1	+ 25.6	0.35	0.86
V3 CNR	245.5	220.4	+ 25.2	0.36	0.83
V3 CBR	1.81	1.56	+ 0.25	0.33	0.82
V3/ICA-C3 ratio	1.02	0.95	+ 0.07	0.39	0.42
V3 decay rate (%)	28.9	28.5	+ 0.4	0.99	0.34

Dominant-type participants (n = 13; 10 left-dominant, 3 right-dominant). Side comparison: Wilcoxon signed-rank test; interaction: two-way repeated-measures ANOVA. No significant dominance effect on the optimal FA was detected (subgroup power limited). CBR, contrast-to-background ratio; CNR, contrast-to-noise ratio; ICA, internal carotid artery; V3, vertebral artery third segment.

Discussion

Returning to the questions posed in the Introduction, our study answers them as follows: (I) peak-SNR/CNR optimization does not identify the FA readers judge best, the SNR-optimal ≈ 16° coincided with the steepest fall in reader score and reader-assessed diagnostic adequacy (100% at 12° → 71.8% at 16° → 41.0% at 18°); (II) reader depiction is tracked not by SNR/CNR but by along-segment continuity (the V3/ICA-C3 ratio and the proximal-to-distal decay rate) which correlated strongly and significantly with reader score (pooled ρ = 0.61 and − 0.62) whereas SNR (ρ = 0.19) and CNR (ρ = 0.12, not significant after clustering) did not and (III) slow-flow V3 diverges from fast-flow segments such as the ICA because its magnetization is saturated by repeated intra-slab excitation at a far lower FA, and this divergence is not significantly modified by vertebral dominance (flip-angle × dominance interaction p = 0.86 for V3 SNR).

Peak or mean SNR, the metric clinicians and physicists instinctively maximize, is a poor proxy for V3 depiction. SNR averages the bright proximal portion of a long slow-flow segment and is blind to distal dropout; reader depiction, by contrast, is a continuity judgement.

In 3D TOF, blood within the slab is continuously repeatedly excited by radiofrequency pulses[1]. A slow-flow V3 parcel is repeatedly excited during its long transit, so its magnetization is progressively saturated (proximal-to-distal decay); a larger FA worsens this at every pulse. The steady-state recursion $M(n) = E \cdot \cos\alpha \cdot M(n-1) + (1-E)$ [14] makes the two effects explicit: the per-pulse tip grows with α while the recovery term (1 − E) is fixed by T1 and TR, so a larger α drives the parcel toward a lower saturated steady state before it reaches the V3 segment. Lowering the FA reduces the per-pulse tip, preserves magnetization deeper into the slab and restores V3 continuity without materially lowering the already-high SNR of fast-flow segments. Based on idealized Bloch-recurrence model [15] (Fig. 6), which predicts that a slow-flow parcel traversing the 50-mm slab retains only ≈ 0.80 of M0 at a 12° center FA, but retains

only ≈ 0.60 at 18°. Our in-vivo measurements track this magnetization-based prediction closely rather than the idealized displayed-signal curve: the measured proximal-to-distal V3 signal loss was 17.9% at 12° and 36.5% at 18°, near the model's Mz loss and far below the idealized signal rise, so the recurrent tipping, not TONE, dictates distal V3 signal. The residual model-to-measurement gap reflects V3's tortuous, slab-oblique course, which attenuates the effective flip-angle ramp and explains why TONE alone cannot rescue distal V3.

Most prior 3D TOF-MRA optimization studies chose FA based on peak signal-to-noise ratio (SNR) or contrast-to-noise ratio (CNR), or maximized the SNR via the Ernst angle [1] [2] [3]. TOF-MRA Flip-angle surveys quantified the vessel SNR and CNR directly and chose the maximized parameters [16], and multiple-flip-angle techniques were justified by statistically significant SNR gains at the carotid bifurcation [17]. Although a few investigations graded image quality qualitatively, the field has largely equated strong signal with good depiction.

Along-segment continuity, not peak SNR/CNR, should be the endpoint for optimizing long slow-flow vessels. The V3/ICA-C3 ratio and the decay rate both tracked reader score strongly (pooled $|\rho| = 0.61$ and 0.62; 95% CIs 0.54–0.68 and − 0.68 to − 0.54, both excluding zero), whereas CBR, which rises monotonically with FA through background suppression, showed only a weak, non-significant association, and CNR showed no significant correlation after clustering adjustment. In this cohort the ≈ 25% decay level coincided with the steepest drop in reader metrics; this observation is hypothesis-generating and requires external validation. We caution against treating 25% as a universal constant. The approximately 25% decay level was identified and evaluated within the same cohort and should not be read as a generalizable cutoff for V3 dropout. Its value shifts with slab thickness, TONE profile and field strength.

V3 is the lesion-bearing portion of the vertebral artery in precisely the posterior-circulation syndromes for which non-contrast 3D TOF MRA is useful. In Bow Hunter's syndrome the symptomatic stenosis localizes to the atlanto-axial V3 [18] [19]; in atherosclerotic vertebral artery disease V3 is a frequent site of symptomatic stenosis contributing to posterior-circulation stroke [20]; and the distal extracranial vessel is the segment of interest in suspected V3 dissection. Our data show the risk is not hypothetical: at routine 18°, V3 decay reached 36.5% and reader-assessed diagnostic adequacy fell to 41.0%, leaving the distal segment non-diagnostic in most examinations. Choosing the FA by continuity rather than peak SNR is expected to protect against this failure mode.

Because lowering the FA only mildly reduces the absolute SNR of fast-flow segments while rescuing V2/V3 continuity, ~ 12° is a favorable compromise for cervical 3D TOF whenever V3 (or other slow-flow) depiction matters. Changing only one parameter is cheap and reversible to restore continuous V3 depiction without measurably harming ICA or V2 depiction. The flip-angle optimization was not significantly modified by vertebral dominance: the dominant side was numerically brighter (SNR difference + 25.6, $p = 0.35$) and the flip-angle × dominance interaction was non-significant for every metric ($p = 0.86$), so a single low FA serves balanced and dominant anatomies alike. As with the

companion, the absolute optimum (here ~ 12°) is scanner- and TONE-profile dependent and should be re-validated per system, consistent with the continuity-based endpoint advanced above. Optimum FA is 12° at which both reader depiction scores and diagnostic adequacy peaked across the full 8°–25° range (Fig. 4). This value bridged the Ernst-equilibrium prediction (~ 9°) and the intra-slab saturation optimum (~ 17°), providing direct empirical support for the Bloch-recurrence model (Fig. 6).

Strengths include strict intra-individual design. Every participant scanned at all eight FAs in randomized order, removing between-subject confounding and providing high paired power for the observed effects (partial η^2 up to 0.90) and blinded dual-reader scoring with excellent agreement (quadratic-weighted κ = 0.98), so the continuity endpoint is unlikely to be a reader idiosyncrasy. There are some limitations in this study. Regions of interest were placed by a single reader, so intra- and inter-reader variability of the quantitative metrics was not quantified, although the within-subject flip-angle comparison is unaffected. This was a single-center, single-vendor 3.0T study; relative flip-angle comparisons are unaffected because all eight acquisitions shared identical conditions, although absolute SNR and depiction vary with scanner, reconstruction, field strength and sequence choice[21, 22]. The TONE profile was fixed at 70%; the absolute optimal FA would shift under a different TONE percentage, but not the direction of the conclusion. Depiction was reader-assessed without a catheter DSA or CE-MRA reference standard [23], so reader-assessed diagnostic adequacy reflects reader judgement of continuity rather than a ground-truth stenosis.

Conclusion

For the slow-flow vertebral artery V3 segment, optimizing FA by peak SNR or CNR is inadequate because these indices ignore intra-slab saturation along the vessel; along-segment continuity quantified by the proximal-to-distal decay or the V3/ICA-C3 ratio and governed by Bloch recurrence is the endpoint that tracks reader depiction. A lower FA (~ 12°) preserves V3 continuity without compromising fast-flow depiction, and the prescription was not significantly modified by vertebral dominance in this cohort. The absolute optimum should be re-validated per scanner and TONE profile; on this 3.0T system with 70% TONE, ~ 12° preserves V3 continuity.

Abbreviations

3D TOF
three-dimensional time-of-flight
VA
vertebral artery
V3
third (extradural) segment of the VA
ICA
internal carotid artery
SNR

signal-to-noise ratio
CNR
contrast-to-noise ratio
CBR
contrast-to-background ratio
FA
flip angle
TONE
tilted optimized non-saturating excitation
rm-ANOVA
repeated-measures analysis of variance
SD
standard deviation
CI
confidence interval

Declarations

Ethics Approval

This study was approved by the Institutional Review Board of the authors' institution (approval number withheld for double-blind review). Written informed consent was obtained from all participants. All procedures were performed in accordance with the 1964 Declaration of Helsinki and its later amendments.

Informed consent

Written informed consent was obtained from all participants.

Competing interests

The authors declare no competing interests.

Funding

This research received no specific grant from any funding agency.

Author Contribution

Guijin Li: Study design, manuscript drafting and revision. Jiewen Qiu: Volunteer recruitment, statistical analysis. Dianjiang Zhao: Subjective image quality scoring. Hongjie Cao: Subjective image quality

scoring. Xiuqin Jia: Manuscript revising and editing. Haishui Xie: Quantitative data analysis. Shuitao Qiu: Data acquisition, image processing.Qi Yang: Overall study design, supervision, and project administration.All authors reviewed and approved the final manuscript.

Data Availability

The datasets generated and analyzed during the current study are not publicly available due to patient privacy and institutional data protection policies, but are available from the corresponding author on reasonable request.

STROBE statement This observational study was reported in line with the STROBE guidelines (item 14a baseline table provided as Table 1).

This manuscript reports a planned companion analysis that shares the prospective 3D time-of-flight MR angiography flip-angle cohort with a manuscript currently under review. The two manuscripts were designed with non-overlapping primary endpoints. The companion's primary question is whether ~ 12° is non-inferior to routine 18° for binary diagnostic adequacy of V3 (n = 30), whereas the present study's primary question is which continuous metric, along-segment continuity versus peak SNR/CNR, should guide flip-angle optimization (n = 38 with complete bilateral V3 quantitative data). Both papers report descriptive diagnostic-adequacy curves for context, but the inferential claims do not overlap. To preclude partitioned publication, a combined analysis of the shared cohort is available from the authors on request.

All authors made substantial contributions to conception and design, data acquisition, analysis and interpretation of data, and to drafting and critically revising the manuscript. The corresponding author had full access to all data and takes responsibility for the integrity of the data and the accuracy of the data analysis. All authors read and approved the final manuscript. Detailed individual contributions are provided on the title page.

References

1. Saloner D. The AAPM/RSNA physics tutorial for residents. An introduction to MR angiography. Radiographics. 1995;15(2):453–65.
2. Wheaton AJ, Miyazaki M. Non-contrast enhanced MR angiography: Physical principles. J Magn Reson Imaging. 2012;36(2):286–304.
3. Edelman RR, Koktzoglou I. Noncontrast MR angiography: An update. J Magn Reson Imaging. 2019;49(2):355–73.
4. Liu J, et al. Histological validation of three-dimensional variable flip angle turbo spin echo multi-contrast magnetic resonance vessel wall imaging in characterizing carotid vulnerable atherosclerotic plaques. J Cardiovasc Magn Reson. 2024;26(2):101112.

5. Atkinson D, et al. Improved MR angiography: magnetization transfer suppression with variable flip angle excitation and increased resolution. Radiology. 1994;190(3):890–4.
6. Nägele T, et al. [MR angiography of the neck vessels with optimized linearly increasing flip angles]. Rofo. 1994;161(5):399–403.
7. Ikushima. I et al. Variable tip angle slab selection pulses for carotid and cerebral time-of-flight MR angiography. Acta Radiologica, 1997. 38(1997)(2): pp. 275–280.
8. Dagirmanjian A, et al. High resolution, magnetization transfer saturation, variable flip angle, time-of-flight MRA in the detection of intracranial vascular stenoses. J Comput Assist Tomogr. 1995;19(5):700–6.
9. Fellner C, et al. Renal arteries: evaluation with optimized 2D and 3D time-of-flight MR angiography. Radiology. 1995;196(3):681–7.
10. Mayer-Suess L, et al. Cervical Artery Tortuosity Is Associated With Dissection Occurrence and Late Recurrence: A Nested Case-Control Study. Stroke. 2025;56(2):413–9.
11. Griffin KJ, et al. Epidemiology of Spontaneous Cervical Artery Dissection: Population-Based Study. Stroke. 2024;55(3):670–7.
12. Schubert T, et al. Attenuation of blood flow pulsatility along the Atlas slope: a physiologic property of the distal vertebral artery? AJNR Am J Neuroradiol. 2015;36(3):562–7.
13. von Elm E, et al. Strengthening the Reporting of Observational Studies in Epidemiology (STROBE) statement: guidelines for reporting observational studies. BMJ. 2007;335(7624):806–8.
14. Ernst RR, Anderson WA. Application of Fourier Transform Spectroscopy to Magnetic Resonance. Rev Sci Instrum. 1966;37(1):93–102.
15. Frahm J, Haase A, Matthaei D. Rapid NMR imaging of dynamic processes using the FLASII technique. Magn Reson Med. 1986;3(2):321–7.
16. Faro SH, et al. Carotid artery bifurcation: multiple-flip-angle, three-dimensional, time-of-flight MR angiographic technique. Radiology. 1998;206(2):555–9.
17. Mohamed FB et al. Multiple flip angle MRA: data acquisition and post-processing. in Proceedings of 17th International Conference of the Engineering in Medicine and Biology Society. 1995.
18. Duan G, et al. Advances in the Pathogenesis, Diagnosis and Treatment of Bow Hunter's Syndrome: A Comprehensive Review of the Literature. Interventional Neurol. 2016;5(1–2):29–38.
19. Zaidi HA, et al. Diagnosis and management of bow hunter's syndrome: 15-year experience at barrow neurological institute. World Neurosurg. 2014;82(5):733–8.
20. Zhang C, et al. Posterior circulation stroke due to vertebral artery disease in the Chinese population. Int J Stroke. 2022;17(7):753–60.
21. Shi Z, et al. Time-of-Flight Intracranial MRA at 3 T versus 5 T versus 7 T: Visualization of Distal Small Cerebral Arteries. Radiology. 2023;306(1):207–17.
22. Mizoshiri T, et al. Non-contrast mDixon MR angiography of the neck: Comparison with time-of-flight MR angiography in normal subjects. Medicine. 2021;100:e28351.

23. Bowen BC. MR Angiography versus CT Angiography in the Evaluation of Neurovascular Disease. Radiology. 2007;245(2):357–61.
24. Lu H, et al. Determining the longitudinal relaxation time (T1) of blood at 3.0 Tesla. Magn Reson Med. 2004;52(3):679–82.

Figures

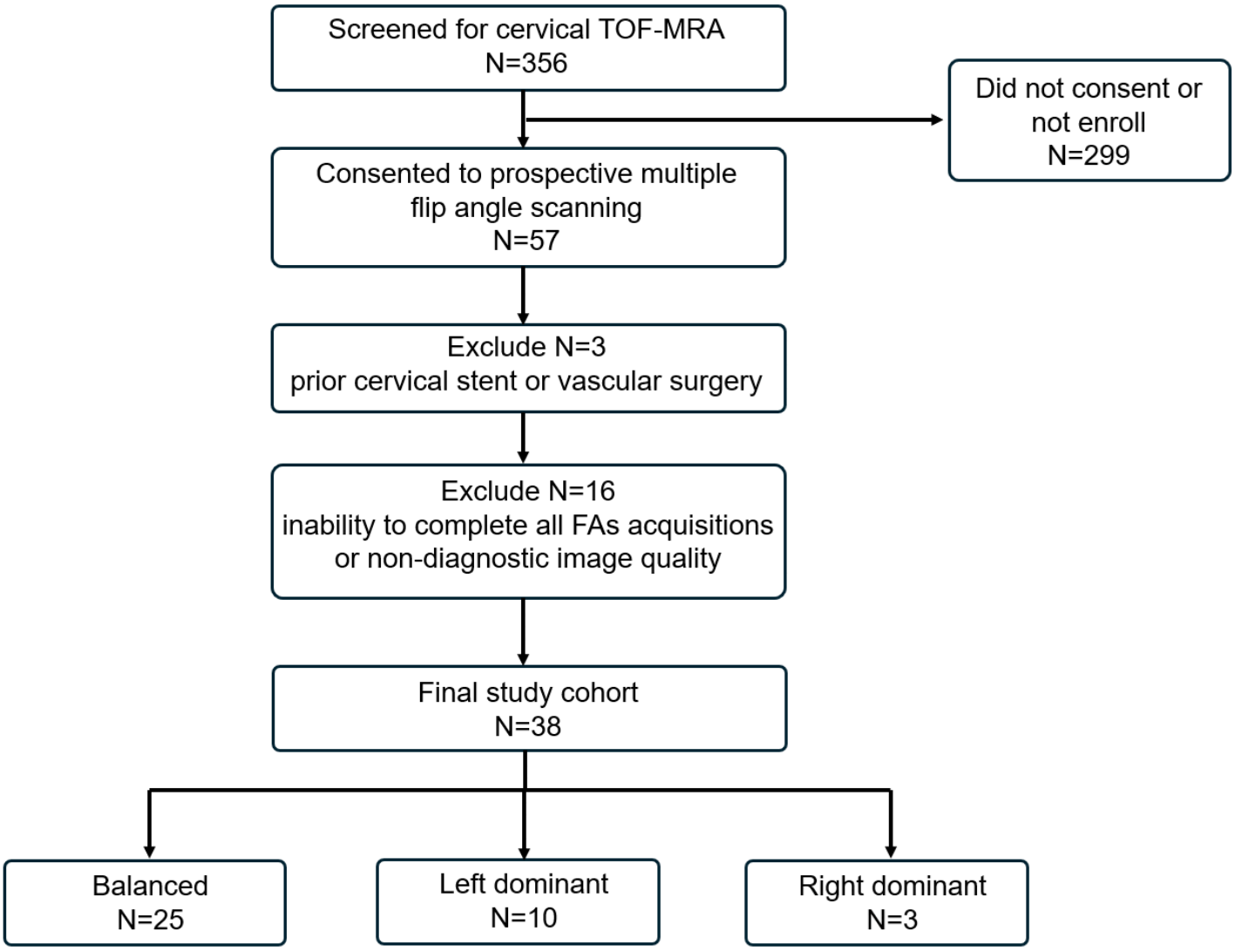


Figure 1

Study flowchart from initial screening to the final cohort of 38 participants, with subdivision by vertebral artery dominance.

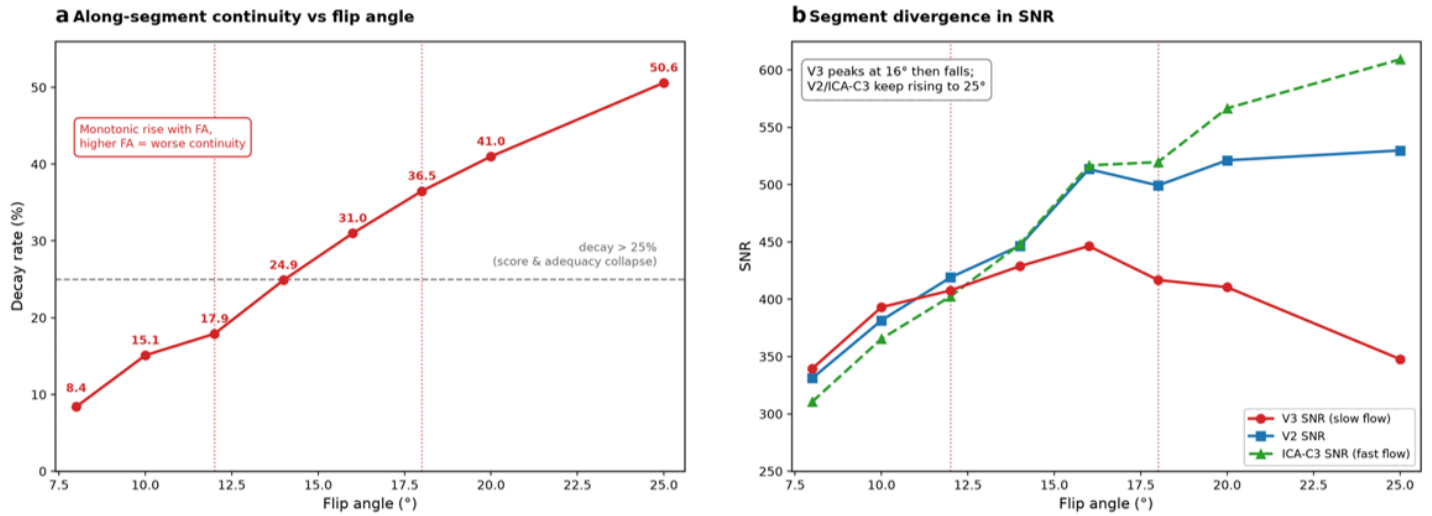


Figure 2

Failure of peak SNR as the optimization endpoint. **a.**V3 proximal-to-distal decay rate versus flip angle, with the cohort-derived ≈25% decay level indicated (exploratory). **b.**SNR of V3 (slow-flow) versus V2 and ICA-C3 (fast-flow): V3 peaks ~16° then falls while the others keep rising.

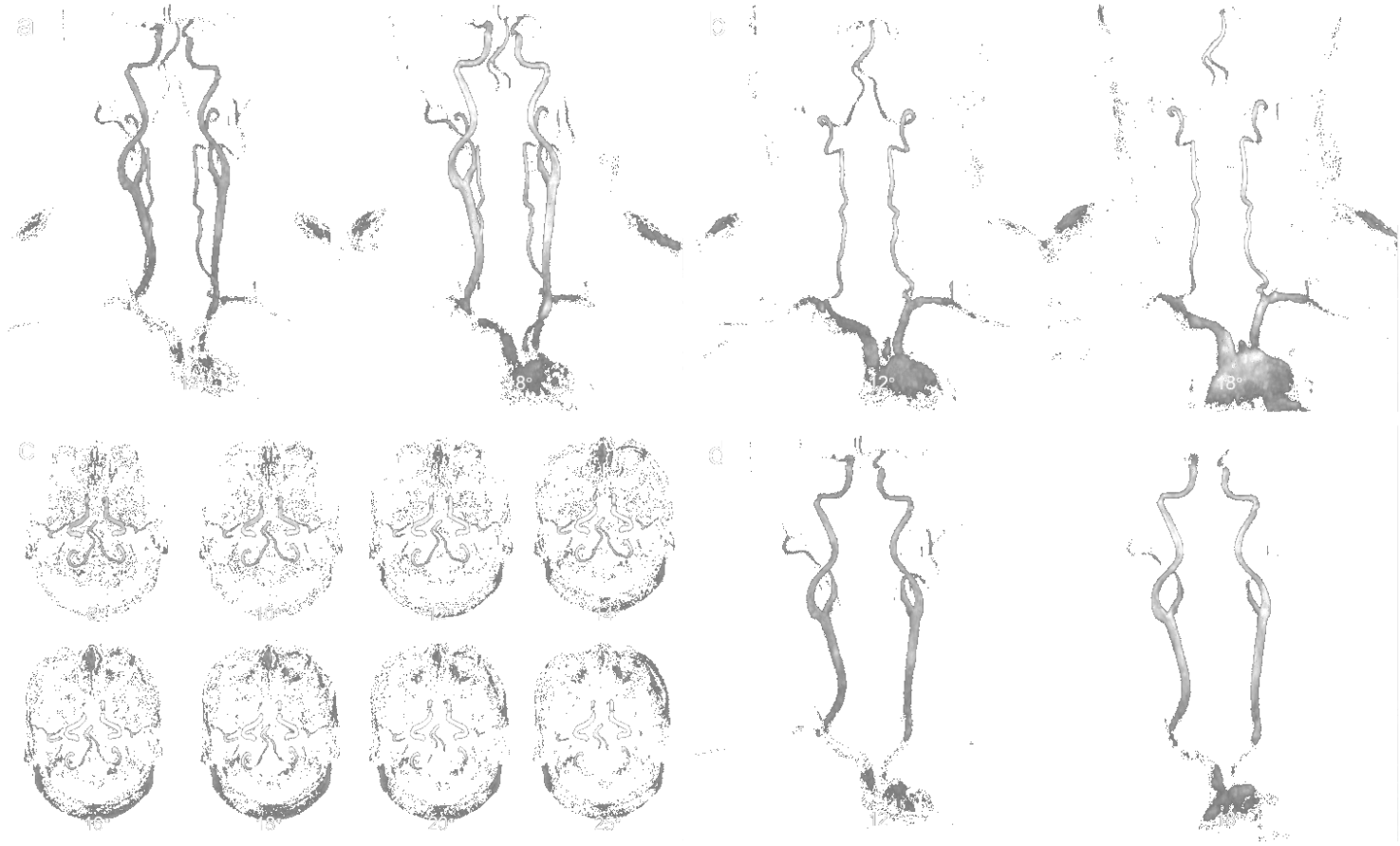


Figure 3

Representative cervical 3D TOF MR angiograms (thick-slab maximum-intensity projections, MIPs) at 12° and 18°. a, b, d Coronal MIPs from three participants, each pair acquired at 12° (left) and 18° (right): at 18° the distal V3 segment loses signal continuity towards the dural entry point, whereas at 12° the V3 segment is depicted continuously from its origin to the dural entry, without degradation of the fast-flow carotid or V2 segments. c Axial MIPs at the level of the skull base in one participant across all eight FAs (8°–25°): intracranial depiction remains diagnostic at every FA, indicating that a low FA does not compromise visualization of the intracranial circulation.

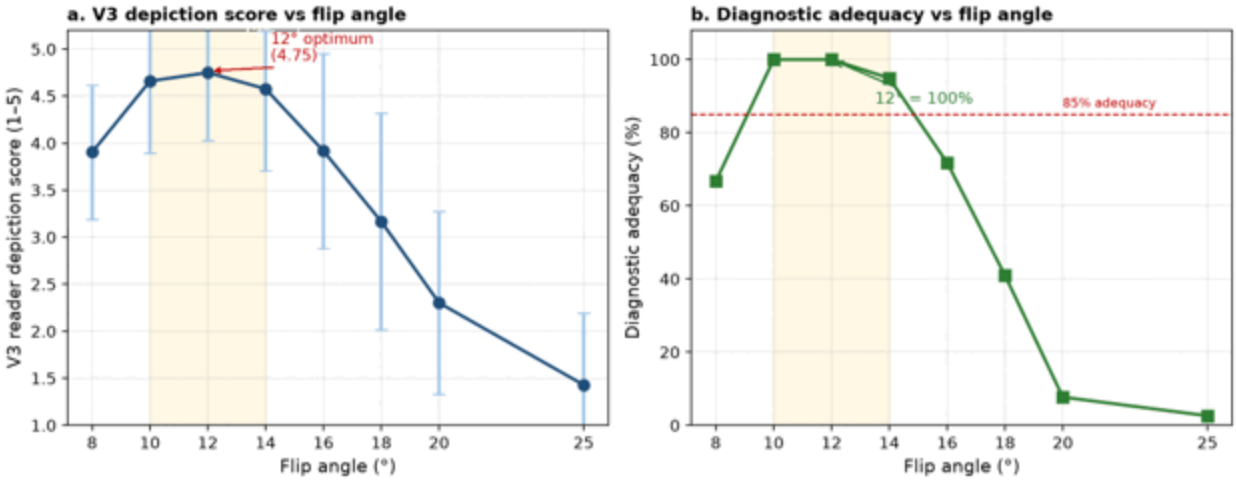


Figure 4

Reader-assessed V3 depiction across the full flip-angle range (8°–25°, n = 38). a V3 reader depiction score (mean ± SD; two blinded raters, both sides pooled) peaked at 12° (4.75 ± 0.72) and declined monotonically at higher angles. b Diagnostic adequacy rated by reader 1 was 100% at 10°–12°, fell below the 85% threshold at 16° (71.8%) and collapsed to 41.0% at 18° and ≤7.7% at ≥20°. Shaded band, acceptable window (10°–14°); dashed line, 85% adequacy threshold.

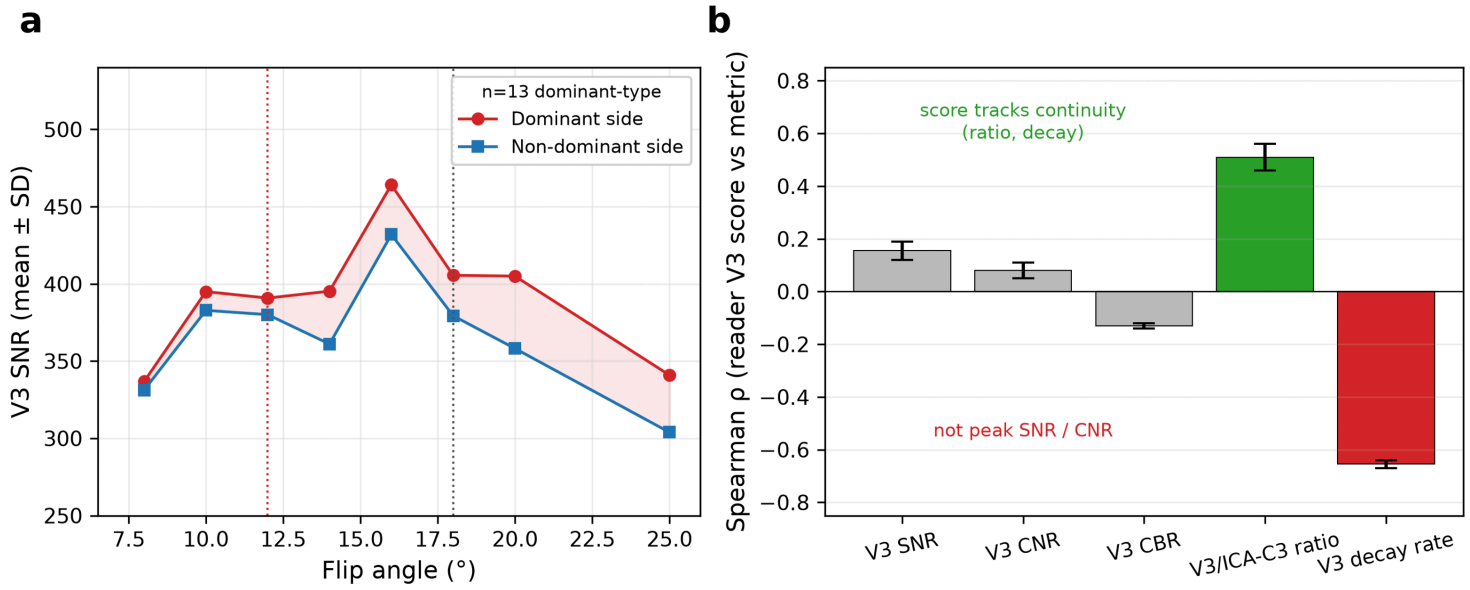


Figure 5

Vertebral dominance and validity of the continuity endpoint. a. V3 SNR by vertebral dominance side across FAs (13 dominant-type participants): no significant side difference was found (side p = 0.35) and the flip-angle × dominance interaction is non-significant (p = 0.86), with no significant interaction detected (subgroup power limited). b. Spearman correlation of reader V3 score with each quantitative metric: the score tracks continuity (V3/ICA-C3 ratio, decay rate) but not peak SNR/CNR or CBR.

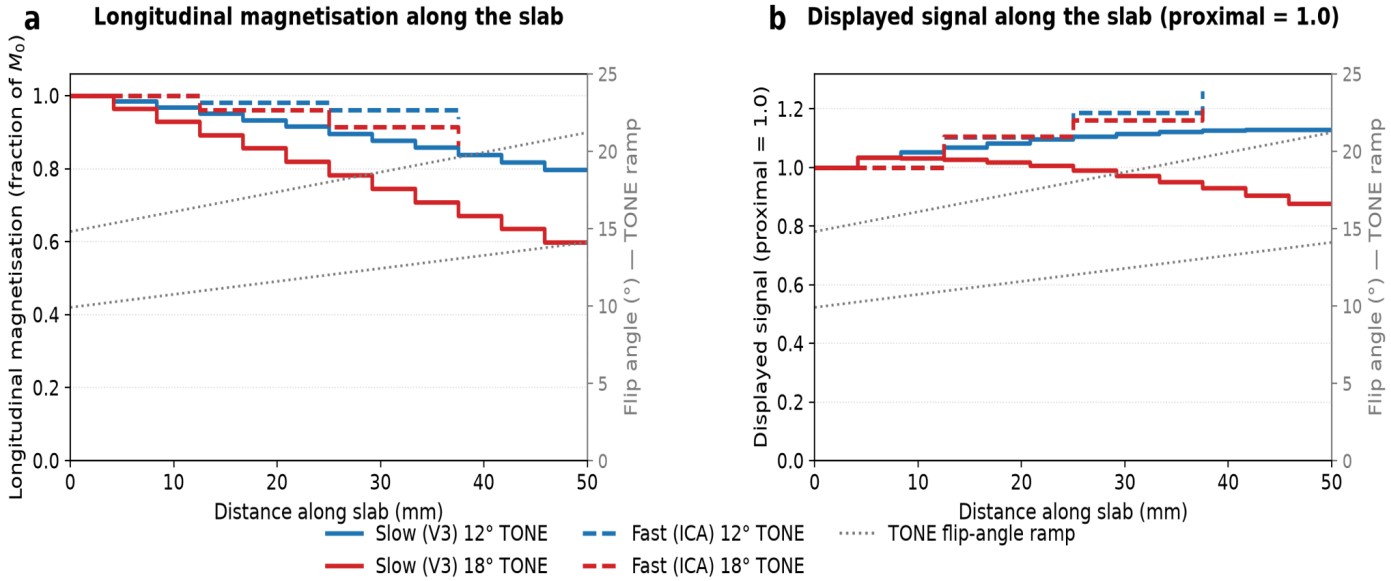


Figure 6

TONE-aware Bloch-recurrence model of intra-slab saturation for slow-flow V3 and fast-flow ICA at 12° and 18° center FAs. Model: blood T1 ≈ 1,664ms at 3.0 T[24], TR = 22ms; a single flowing parcel is excited once per TR while traversing the 50-mm slab, so distal Mz is governed by the cumulative product of cos α and is almost unaffected by TONE (V3 distal Mz ≈ 0.80 at 12°, ≈ 0.60 at 18°; ICA ≈ 0.94 and ≈ 0.86), because T1 (≈1,664ms) ≫ TR (22ms) leaves only minimal inter-pulse recovery and the fast-flow ICA is excited only ≈ 3 times. a. Remaining longitudinal magnetization (fraction of M0) along the slab. b. Displayed signal normalized to the proximal value (= 1.0). In the idealized single-parcel model the TONE flip-angle ramp (grey dotted; 12°: 9.9→14.1°, 18°: 14.8→21.2°) boosts the distal signal and the solid curves rise. Empirically, however, V3 in the present study showed a residual proximal-to-distal signal loss of 17.9% at 12° and 36.5% at 18° , which is much smaller than the idealized single-parcel model predicts and parallels the Mz loss in panel a. The tortuous, slab-oblique course of V3 blunts the effective flip-angle ramp; TONE therefore cannot rescue V3, and a low FA remains necessary. The model is idealized and serves as a mechanistic illustration rather than a patient-specific prediction.

Supplementary Files

This is a list of supplementary files associated with this preprint. Click to download.

- ManuscriptContinuitySupplementarymaterial.docx